Deep-Sea Research I 58 (2011) 647–657

Contents lists available at ScienceDirect

Deep-Sea Research I

journal homepage: www.elsevier.com/locate/dsri

Inferring upwelling rates in the equatorial Atlantic using ^{7}Be measurements in the upper ocean

David Kadko *, William Johns

University of Miami/RSMAS, 4600 Rickenbacker Causeway, Miami, FL 33149, USA

ARTICLE INFO

Article history:
Received 27 October 2010
Received in revised form
11 March 2011
Accepted 15 March 2011
Available online 26 March 2011

Keywords:
Upwelling
Tropical Atlantic
Ocean tracers
Ocean mixing
Radioisotopes

ABSTRACT

Ocean upwelling rates are difficult to measure because of the relatively small velocities involved, and therefore are typically inferred from indirect methods such as heat budget estimates or tracer observations. Here we present the first results using a novel technique, based on the isotope ^{7}Be, to infer rates of upwelling along the equator. Beryllium-7 (half-life=53.3 d) is a cosmic-ray produced radioactive nuclide that is deposited by rainfall upon the ocean surface and subsequently enriched and homogenized within the mixed layer. Previous investigations have utilized the penetration of characteristically high mixed layer concentrations into the upper thermocline to trace ocean ventilation and subduction over seasonal timescales. Here, the tracer is used in a reverse sense; that is, the ^{7}Be concentration in the usually ^{7}Be-rich surface mixed layer will be diluted from penetration of ^{7}Be "dead" water upwelled from below. This dilution provides a means to infer upwelling rates. Furthermore, with knowledge of upwelling rates, ^{7}Be profiles can be used to constrain vertical diffusivity within the upper thermocline. These ideas were tested with samples collected during the Tropical Atlantic Climate Experiment (TACE) cruise (May 22–June 27, 2009). The observations indicated a nearly linear relationship between ^{7}Be inventory and mixed layer temperature, as with increased upwelling, lower mixed layer temperatures correspond to greater ^{7}Be dilution from depth. With this data, upwelling rates were estimated at a number of stations near the equator between 0°E and 30°W within and adjacent to the equatorial cold tongue. The derived upwelling rates ranged from 0 to 2.2 m/d, with maximum values found between the equator and 2°S. The corresponding K_z values derived for the upper thermocline were in the range 1–4 $\times 10^{-4}$ m^2/s.

© 2011 Elsevier Ltd. All rights reserved.

1. Introduction

Upwelling is an important component of the global ocean circulation, which affects biogeochemical cycling, climate dynamics, and sea-surface temperature. Determination of upwelling rates by direct measurement is difficult because of the relatively small velocities involved, and they must therefore be inferred by indirect methods such as those provided by tracer observations. Such tracers derive from the presence, in surface water, of properties characteristic of thermocline water, which have been emplaced by the upwelling process. Examples include surface anomalies in ^{14}C, δ^{13}C, AOU (apparent oxygen utilization), δ^{3}He, pCO_2, ΣCO_2, and temperature (Broecker and Peng, 1982; Broecker et al., 1978; Quay et al., 1983; Wanninkhof et al., 1995; Klein and Rhein, 2004; Rhein et al., 2010). Several of these properties have been used to constrain rates of upwelling. For example, the maintenance of a CO_2 anomaly in the equatorial surface ocean in the presence of gas evasion and plant production demands that upwelling rates be at least tens of meters a year (Broecker and Peng, 1982). However, uncertainties with respect to gas exchange, primary production, and an air–sea equilibration time of ~1year limit the effectiveness of CO_2 for analyzing local and time-dependent upwelling rates. In another example, the helium isotopic disequilibrium (excess δ^{3}He) in the mixed layer of upwelling regions can only be maintained by upward vertical motion, and was used to derive values of vertical velocity in the range of ~1–2 m/d for the equatorial Atlantic (Klein and Rhein, 2004; Rhein et al., 2010), comparable to calculations based on the Ekman divergence for that area (Xie and Hsieh, 1995). The timescale of gas transfer (days) allows this tracer to analyze local upwelling but relies on accurate assessment of the gas exchange rate and vertical diffusivity at the base of the mixed layer.

Here, a novel technique based on the isotope ^{7}Be is used to infer rates of upwelling. Be-7 is a cosmic-ray produced isotope (half-life=53.3 d) that is deposited upon the ocean surface primarily by rainfall and subsequently homogenized within the surface mixed layer (e.g. Silker, 1972; Aaboe et al., 1981;

* Corresponding author. Tel.: +1 305 421 4721.
E-mail addresses: dkadko@rsmas.miami.edu (D. Kadko), bjohns@rsmas.miami.edu (W. Johns).

0967-0637/$ - see front matter © 2011 Elsevier Ltd. All rights reserved.
doi:10.1016/j.dsr.2011.03.004

Young and Silker, 1980; Kadko and Olson, 1996; Kadko, 2000, 2009). In the absence of physical removal processes other than radioactive decay the water column inventory of the isotope represents an integration of the atmospheric input flux over approximately the previous mean-life (77 d) of the isotope.

Typically, penetration of the characteristically high mixed layer concentrations of ^{7}Be into the upper thermocline has been used to trace ocean ventilation and subduction (of water mass, heat, and chemical properties) over seasonal timescales within numerous ocean regimes (e.g. Kadko and Olson, 1996; Kadko, 2000; Kadko and Swart, 2004; Kadko and Johnson, 2008). In these works, the penetration of high ^{7}Be below the mixed layer is used to infer ventilation rates of water that had previously been near the surface within the timescale of the isotopic mean life of 77 d, and derive mixing rates between the mixed layer and the upper thermocline. Here, a method is described how the tracer can be used in a reverse sense; that is, the ^{7}Be concentration in the usually ^{7}Be-rich surface mixed layer will be diluted from penetration of ^{7}Be "dead" water upwelled from below. This dilution provides a means to infer upwelling rates. Furthermore, with knowledge of upwelling rates, ^{7}Be profiles can be used to constrain vertical diffusivity within the upper thermocline. These ideas were tested during a cruise to the equatorial Atlantic in June 2009 as part of the Tropical Atlantic Climate Experiment (TACE).

2. Methods

Samples were collected during the *R/V Endeavor* (cruise EN463, May 22–June 27, 2009) at a total of 19 stations along the cruise track (Fig. 1), mostly along three cross-equatorial sections at 23°W, 10°W, and 0°E. The subsequent analysis followed procedures described in detail elsewhere (Kadko, 2009). Briefly, ^{7}Be was collected at selected depths by pumping 400–700 L of seawater via a 1.5 inch hose into large plastic barrels on deck. From these barrels, the seawater was then pumped through iron-impregnated acrylic fibers at ~10 L/min (Lal et al., 1988; Krishnaswami et al., 1972; Lee et al., 1991). The efficiency of the fiber for extraction of Be from seawater was determined by adding 500 ml of a 1000 ppm Be atomic absorption standard to a drum containing seawater. The seawater was pumped through an iron fiber cartridge and at every 100 L the Be content of the cartridge effluent was measured by atomic absorption. From this data, the integrated Be extraction efficiencies were calculated. For sample volumes in the range 400–700 L, the extraction efficiencies were respectively 82–76%. On land, the fibers were dried and then ashed. The ash was subsequently pressed into a pellet (5.8 cm diameter) and placed on a low background germanium gamma detector.

The ^{7}Be has a readily identifiable gamma peak at 478 keV. The detector was calibrated for the pellet geometry by adding a commercially prepared mixed solution of known gamma activities to an ashed fiber, pressing the ash into a pellet, and counting the activities to derive a calibration curve. The uncertainty of the extraction efficiency (4%) and the detector efficiency (2%) was in all cases smaller than the statistical counting error and the uncertainty in the blank.

Th-234 samples were collected by pumping seawater into 10 L plastic jugs. The samples were then acidified with HCl and spiked with a yield tracer (Th-230) and an iron chloride solution. After equilibrating overnight, thorium was co-precipitated with $FeOH_3$ by adding a sodium hydroxide solution. The precipitate was filtered and then passed through ion exchange columns to remove uranium (Bhat et al., 1969). The Th was electroplated on stainless steel planchets (Anderson and Fleer, 1982) and counted on calibrated alpha and beta detectors.

Particle samples were collected by passing 200 L seawater samples through 142 mm GF/F filters by vacuum filtration. The filters were leached with boiling HCl and HNO_3 in the presence of stable Be and ^{230}Th spikes. The leachate was precipitated with iron hydroxide, dried in a petri dish, and placed on the gamma detector for ^{7}Be analysis. Subsequently, the dried precipitate was dissolved in 1 N HCL. An aliquot of this was used for analysis of stable Be, by AA, to determine the ^{7}Be recovery. The remainder was treated for ^{234}Th analysis as described above.

3. Results and discussion

The ^{7}Be data are presented in Table 1. At each station, a full depth CTD cast was also performed, so that the corresponding temperature profile and mixed layer depth are known. Surface mixed layer ^{7}Be samples were collected at all 19 stations, and at 9 of the stations (which we refer to as "profile" stations), ^{7}Be samples were collected at 4 additional depths within the upper thermocline. The purpose of these profile stations was to estimate the total water column inventory of ^{7}Be at a number of sites where strong upwelling was anticipated to be taking place, as well as at a few locations where upwelling was expected to be weak or zero.

The ^{7}Be activity in the mixed layer (Tables 1 and 2) exhibits a total variation of about a factor of four, between low values of ~200 dpm/m^3 found in areas with cooler sea surface temperatures (SSTs) and high values of ~800 dpm/m^3, which are

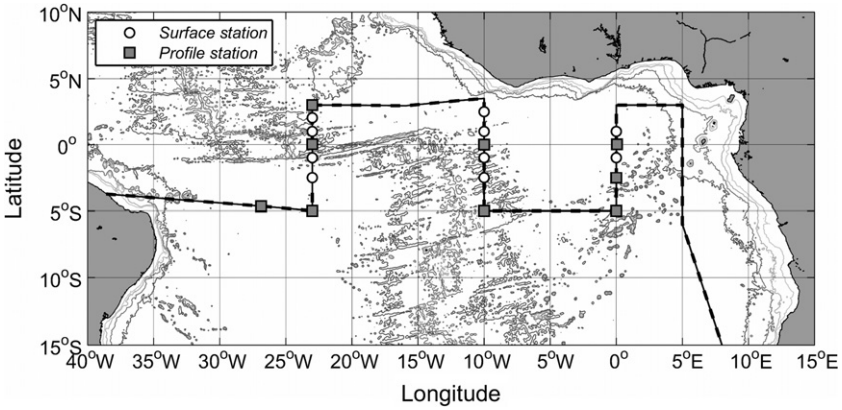

Fig. 1. Cruise track for the *R/V Endeavor* (cruise EN463, May 22–June 27, 2009) indicating location of the ^{7}Be samples (mixed layer samples only, circles; full profiles, squares).

Table 1
^{7}Be water column data.

Station	Lat.–Long.	Depth (m)	^{7}Be (dpm/1000 L)[a]	ML temp.[b]
Sta001	4°39.415′S	15	837 ± 43	29.11
4°S	26°49.000′W	45	101 ± 20	
		75	8.3 ± 22.4	
		110	4.8 ± 12.6	
		125	bd	
Sta002	5°01.294′S	11	739 ± 41	28.95
5°S	23°00.133′W	45	171 ± 28	
		76	44.3 ± 19.6	
		110	bd	
		145	bd	
Sta007	2°31.130′S	15	597 ± 37	29.00
2.5°S	23°00.856′W			
Sta011	0°59.528′S	7	369 ± 35	28.78
1°S	22°59.490′W			
Sta014	00°00.096′N	9	343 ± 26	28.10
0°	22°58.339′W	40	211 ± 22	
		70	bd	
		104	12.5 ± 25.7	
		137	bd	
Sta017	01°00.601′N	9	394 ± 36	28.2
1°N	23°01.232′W			
Sta020	02°02.743′N	18.5	410 ± 44	28.31
2°N	23°00.650′W			
Sta022	03°00.253′N	15	556 ± 40	29.00
3°N	23°00.121′W	45	175 ± 30	
		78	21.2 ± 20.3	
		112	bd	
		144	bd	
Sta028	02°29.571′N	22	1049 ± 68	29.10
2.5°N	10°00.014′W			
Sta032	01°00.305′N	15	784 ± 61	28.37
1°N	10°01.112′W			
Sta035	00°00.532′N	7	297 ± 23	26.31
0°	09°59.418′W	33	123 ± 14	
		64	24.5 ± 14.0	
		100	bd	
		145	bd	
Sta038	00°59.954′S	10	216 ± 36	26.09
1°S	09°59.861′W			
Sta043	2°30.206′S	15.5	243 ± 37	25.81
2.5°S	10°00.482′W			
sta048	5°00.226′S	15	327 ± 36	26.96
5°S	09°59.680′W	68	113 ± 20	
		87	9.8 ± 19.8	
		110	bd	
		134	bd	
Sta051	4°59.642′S	17	312 ± 38	26.67
5°S	00°0.063′W	60	32.0 ± 31.8	
		90	8.2 ± 12.9	
		113	–	
		154	4.6 ± 27.7	
Sta056	2°29.989′S	12	178 ± 38	25.47
2.5°S	0°00.921′W	39	13.7 ± 23.6	
		63	3.0 ± 18.5	
		104	bd	
		146	bd	
Sta060	0°59.054′S	17.6	270 ± 39	25.5
1°S	0°00.711′E			
Sta064	0°01.679′N	16	368 ± 41	27.16
0°	0°03.801′W	42	61.4 ± 26.4	
		76	18.8 ± 16.0	
		106	bd	
		132	bd	
Sta068	0°59.967′N	15	432 ± 45	27.42
1°N	0°00.311′W			

bd = below detection.

[a] dpm = 60 bq;
[b] ML = mixed layer.

associated with warm SSTs. The cooler temperatures along the equator are associated with the seasonal development of the equatorial cold tongue in April–May, as easterly winds increase along the equator and drive upwelling through enhanced surface Ekman divergence. The decrease in mixed layer ^{7}Be activity with decrease in temperature occurs as ^{7}Be-"dead", cold water is upwelled from below. Profiles comparing temperature and ^{7}Be from upwelling and adjacent non-upwelling stations clearly show the deficit of ^{7}Be in the upwelling water column where deep colder water reaches the surface (Fig. 2, Table 2). The point made here is that the "deficit" of the ^{7}Be inventory relative to the non-upwelling stations can provide a measure of the upwelling rate.

3.1. Estimating upwelling rates from ^{7}Be profile data

We consider a model of the upper ocean consisting of a surface mixed layer with constant ^{7}Be concentration (C_0), and an underlying "tail" layer where the ^{7}Be concentration decays $C(z)$ to zero at some depth z_0 (Fig. 3). This depth was typically of the order of 70 m, while the corresponding mixed layer depths varied from about 10 to 40 m.

Under the assumption of steady state, and neglecting horizontal advection (see Appendix), an equation can be formed that relates the upwelling at the base of the mixed layer (w_H) to the total water column ^{7}Be inventory (C_{inv}):

$$w_H C_0 = F - \lambda C_{inv} + \int_{z_0}^{H} C(z)\frac{\partial w}{\partial z}dz \quad (1)$$

where

$$C_{inv} = \int_{z_0}^{0} C(z)dz = C_0 H + \int_{z_0}^{H} C(z)dz$$

Here F is the ^{7}Be surface flux into the mixed layer, λ is the ^{7}Be decay constant, and H is the mixed layer depth. If the vertical velocity is assumed to be uniform between the base of the mixed layer and the depth z_0 where the ^{7}Be signal decreases to zero, then (1) becomes

$$w_H = \frac{1}{C_0}(F - \lambda C_{inv}) \quad (2)$$

In the case where upwelling is negligible, (1) is simply

$$F = \lambda C_{inv}$$

which represents a balance between the atmospheric input of ^{7}Be to the ocean and its radioactive decay. Thus, the water column inventory (i.e. the depth integrated decay) of ^{7}Be at non-upwelling stations can be used to estimate the regional surface ^{7}Be flux. In this manner the control flux F (dpm/m^2) determined by the water column inventory of non-upwelling stations serves as the regional atmospheric flux and anchors the relationship. This flux will differ regionally, but within narrow regional locations, the use of a control flux as representative of the atmospheric input for that region is a reasonable assumption. For this study we used the average atmospheric input obtained from our stations 1 and 2, which were taken near 5°S and 25°W, to the west and south of the main upwelling region.

This assessment of upwelling does not require consideration of vertical mixing because we are concerned only with the integrated inventory of ^{7}Be over the mixed layer and the upper thermocline (the "box" illustrated in Fig. 3). Vertical mixing is internal to this box and will influence the shape of the ^{7}Be profile (see Section 3.2). For example, if vertical mixing is weak, then the tail layer will be thin and most of the ^{7}Be inventory will be contained in the mixed layer. In the limit of no vertical mixing, and a vanishing tail layer (see Appendix), (2) reduces to

Table 2
Inventories and box model calculation.

Station	ML temp. (°C)	ML ^{7}Be (dpm/m^3)	ML depth (m)	^{7}Be inventory (dpm/m^2)	Apparent flux (dpm/m^2/d)	Fraction ^{7}Be inventory	W (m/d)
001	29.11	837	31	35,320	459	1	0.0
002	28.95	739	35	34,500	449	1	0.0
014	28.10	343	20	18,460	240	0.53	0.62
022	29.0	556	34	25,284	329	0.725	0.225
035	26.31	297	10	10,111	131	0.29	1.09
048	26.96	327	55	22,064	282	0.63	0.53
051	26.67	312	40	15,909	207	0.46	0.79
056	25.47	179	20	5232	68	0.15	2.16
064	27.16	368	20	12,835	167	0.37	0.78

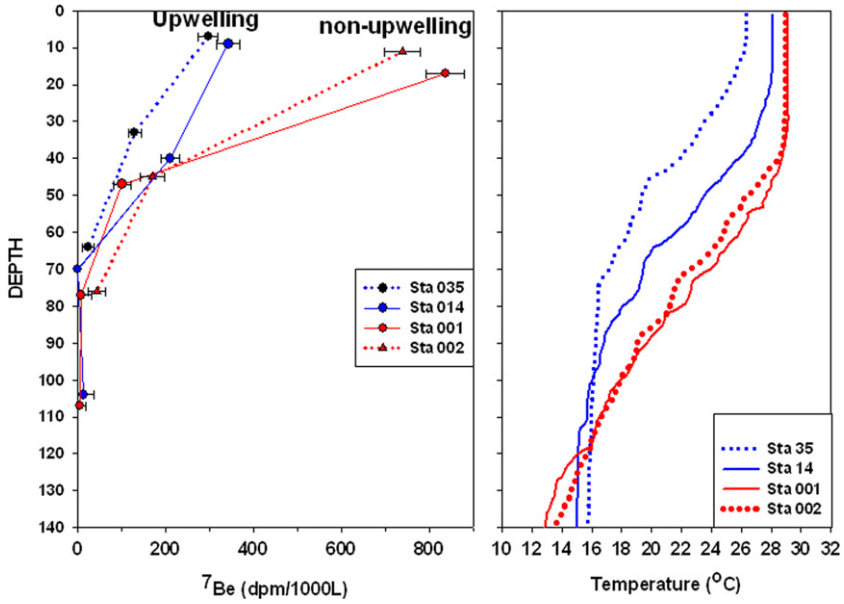

Fig. 2. ^{7}Be and temperature profiles for upwelling (blue) and non-upwelling stations (red) from the TACE expedition along the equatorial Atlantic. Note that the cold, upwelled water corresponds to lower water column ^{7}Be.

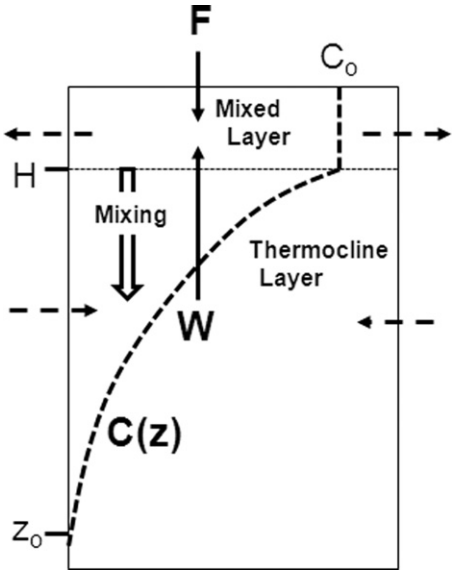

Fig. 3. Conceptual model used in upwelling calculation. C_0=[^{7}Be] mixed layer, C_{z0}=[^{7}Be] at depth=Z_0, W=constant upwelling velocity through the upper thermocline (m/d), and H=depth of mixed layer. The dashed line is the ^{7}Be concentration profile ($C_{(z)}$) internal to the box comprising the mixed layer and the upper thermocline. The dashed arrows indicate relative divergence of horizontal flow in the mixed layer and the convergence in the thermocline.

the "slab" model:

$$w_H = \frac{1}{C_0}(F - \lambda C_0 H) \tag{3}$$

which permits a qualitative estimate of the upwelling strength from just the mixed layer ^{7}Be concentration.

^{7}Be inventories were calculated at the profile stations by assuming uniform concentration in the mixed layer, and fitting a shape-preserving (Akima) cubic spline to the ^{7}Be data in the upper thermocline. The mixed layer depth H was taken from the corresponding temperature profiles, defined as the depth where the temperature changes from its surface value by 0.5 °C (Hayes et al., 1991). The ^{7}Be inventories and the calculated upwelling rates, using Eq. (2), are presented in Table 2 and plotted against mixed layer temperature in Fig. 4. With decrease in temperature the inventory decreases, as the calculated upwelling rates increase, as would be expected. The range of w_H calculated from the ^{7}Be deficit, 0–2.2 m/d, is comparable to the few available results using other methods for this region (e.g. Xie and Hsieh, 1995; Klein and Rhein, 2004; Rhein et al., 2010), and with typical values found in the Pacific equatorial cold tongue region (e.g. Wang and McPhaden, 1999).

Uncertainties in the upwelling estimates due to the neglect of horizontal advection of ^{7}Be can be evaluated based on the observed horizontal gradients of ^{7}Be and typical magnitudes of surface velocities in the region. For example, in Eq. (3) there

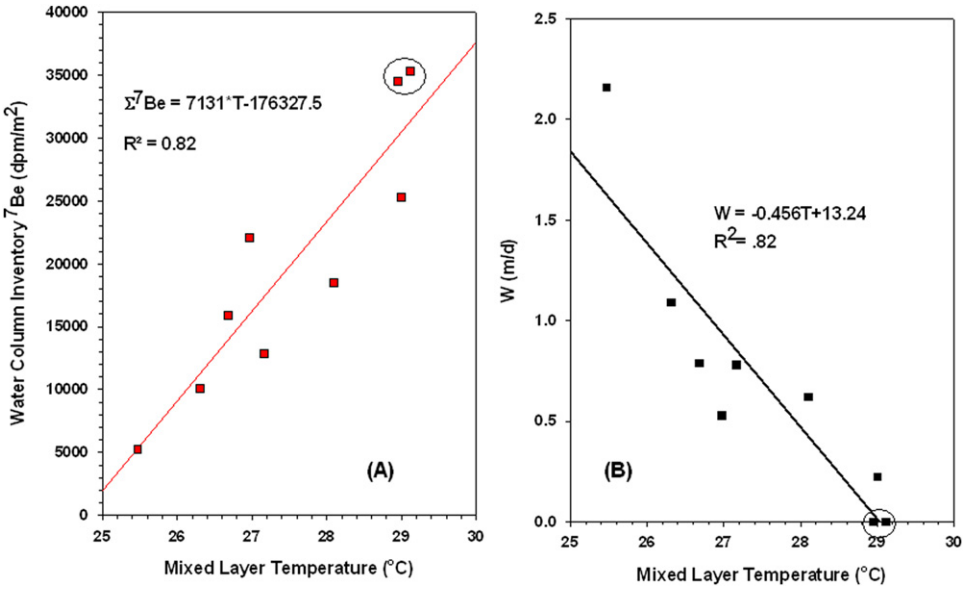

Fig. 4. (A) The ^{7}Be inventory and (B) the calculated upwelling rate (W) plotted against mixed layer temperature from the TACE expedition along the equatorial Atlantic. The circled points are from the warm, non-upwelling stations.

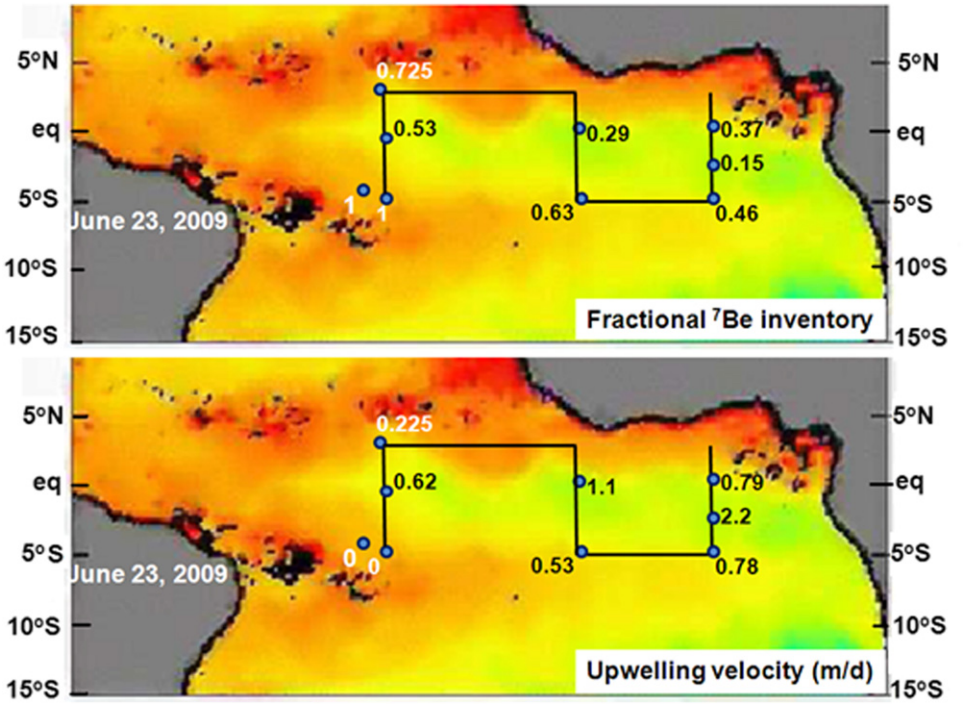

Fig. 5. Station track superimposed over SST for June, 2009. (A) ^{7}Be inventories, as a fraction of the control flux, ($F=1$), are indicated. (B) The derived upwelling velocities (W, Eq. (2)) are indicated. The relationship between the inventories, W, and SST is clearly seen.

would be a term $-H(u_0\partial C_0/\partial x+v_0\partial C_0/\partial y)$ on the right hand side (see Appendix), and the uncertainty in w_H caused by this can be estimated by comparing this term to the size of the atmospheric flux F. Along the equator, in the band of minimum ^{7}Be concentration, meridional advection is negligible ($\partial C_0/\partial y\sim 0$) and zonal gradients of the mixed layer ^{7}Be are weak, of the order 0.05 (dpm/m^3)/km, leading to uncertainties of the order (10–15%) in w_H for typical zonal velocities of 0.5 m/s (Lumpkin and Garzoli, 2005). Off the equator, meridional gradients of ^{7}Be become relatively large, of the order 0.5 (dpm/m^3)/km, and with typical off-equatorial meridional velocities of 0.1 m/s the errors can reach 30%. The tendency of this advection is to spread the ^{7}Be depleted waters from the equator, poleward, resulting in an overestimate of upwelling for off-equator sites. Thus, we conclude that the near-equatorial upwelling estimates, in the areas where upwelling is the strongest, are not significantly affected by horizontal advection, but that accurate estimates in the off-equatorial regions will normally require taking horizontal advection into account.

In Fig. 5, the station track is superimposed over SST for late June 2009. The SST data were obtained from the NASA Tropical Rainfall Measuring Mission (TRMM) TMI weekly-averaged satellite sea surface temperatures (http://www.remss.com/tmi). In Fig. 5A the ^{7}Be inventories are plotted with the control inventory

stations from the non-upwelling sites (warmest water) normalized such that their inventories are 1. The other sites have some fraction of that inventory (<1). The corresponding upwelling velocities are shown in Fig. 5B. Despite the slower response time of the ^{7}Be signal relative to SST, the relationships between decreasing ^{7}Be inventories, higher w_H, and lower SST described graphically in Fig. 4 are clearly seen.

As discussed in the Appendix, the w_H estimate derived from Eq. (2) is a lower bound, as the actual w_H will be higher if the upwelling velocity is not constant, as assumed, but decreases with depth. The last term in (1) is then non-zero and positive, and can be estimated given an assumed structure of $w(z)$. Taking the simplest case, where w decreases linearly to zero over a depth scale z_w below the mixed layer (e.g. Quay et al., 1983), $dw/dz = w_H/z_w$ in Eq. (1) and the resulting w_H is

$$w_H = (F-\lambda C_{inv}) \Big/ \left[C_0 - \frac{1}{z_w}\int_{z_0}^{H} C(z)dz\right] \quad (4)$$

The three different values of w_H obtained from Eqs. (2)–(4) are listed in Table 4 and compared in Fig. 6, where in (4) we have used a decay scale for w of $z_w=100$ m. This is a reasonable assumption based on inferences from observations and model results in the equatorial regions (e.g. Harrison, 1996). The slab mixed layer model estimates (Eq. (3)) tend to be the largest, and exceed the inventory method estimates (Eq. (2)), by $35\pm25\%$ on average. The variable w estimates (Eq. (4)) are intermediate between the mixed layer (slab) and the inventory method estimates for the lower range of upwelling rates and tend to exceed the mixed layer model estimates at higher upwelling rates. On average the variable w estimates are larger than the inventory method estimates by $21\pm15\%$. We believe the variable w estimates are probably the most realistic, and so the inventory method values are likely to underestimate the actual upwelling rate by $\sim$20%. Interestingly, the average difference between the slab mixed layer model estimate and the variable w estimate is only $8\pm12\%$, so that the slab model estimate, though based on an unrealistic assumption of zero vertical mixing, provides a reasonable estimate of the upwelling rate even though it relies on only a single measurement of the ^{7}Be in the mixed layer.

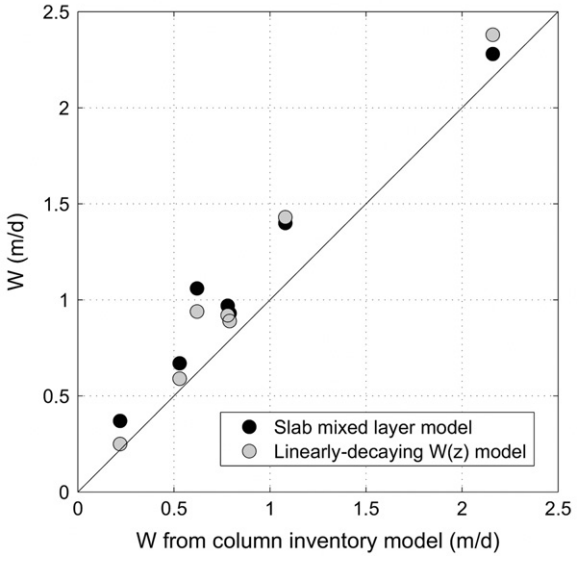

Fig. 6. A comparison of upwelling rates derived from the inventory model (Eq. (2)) to those derived from the slab mixed layer model (Eq. (3)) and the linearly decaying $W(z)$ model (Eq. (4)).

3.1.1. Potential complications

Two potential complications must be considered here. One is the possible particle removal of ^{7}Be from the surface ocean, which would tend to enhance the calculated upwelling velocity. The other is variability of the input flux (F) across the study area.

In regards to particle scavenging, ^{7}Be is considered a conservative tracer in the open ocean regime. Numerous studies have shown that ^{7}Be is quite soluble in the relatively low particle environment of the open ocean, thus allowing particulate transport to be ignored. Silker (1972) found that $<10\%$ of ^{7}Be was on the insoluble fraction in the water column during his study at Bermuda. Aaboe et al. (1981) measured ^{7}Be in the western Sargasso Sea and found that the calculated standing crop in the Sargasso Sea is equal to that predicted from precipitation collectors, as have Kadko and Prospero (2011) from the same area. Recently, to test the extent to which ^{7}Be is associated with marine particles, Andrews et al. (2008) pumped $\sim$1000 L of seawater through a 1 μm Hytrex filter from surface water of the Sargasso Sea and found that the particulate matter had a ^{7}Be activity below the detection limit. Here, ^{234}Th in the water column and particulate ^{7}Be and ^{234}Th were measured to determine the degree to which ^{7}Be might be scavenged from particles in more biologically productive regions associated with upwelling. Th-234 is a naturally occurring, highly particle-reactive radioisotope ($T_{1/2}=24.1$ d) that is widely used to study particle removal and associated elemental export rates from the surface ocean on timescales of days to weeks. Briefly, the degree of radioactive disequilibrium between ^{234}Th and its parent ^{238}U in the upper ocean yields a measure of the scavenging removal of the particle-reactive Th from the surface to depth (e.g. Matsumoto, 1975; Coale and Bruland, 1985, 1987; Bruland and Coale, 1986). In the simple formulation, the particle removal flux, P_{Th}, of ^{234}Th is proportional to the integrated ^{234}Th deficit in the upper ocean:

$$P_{Th} = \Sigma(^{238}U - ^{234}Th)\lambda_{Th}\Delta z \quad (5)$$

where λ_{Th} is the decay constant of ^{234}Th, ^{234}Th and ^{238}U are isotope concentrations, and Δz the depth interval between samples. The observed deficiency of ^{234}Th (P_{Th}) can be used to determine the scavenging removal of other elements (e.g. Bruland and Coale, 1986; Buesseler et al., 1992, 1995; Weinstein and Moran, 2005). Thus, removal of ^{7}Be by particle scavenging, P_{Be}, can be related to ^{234}Th removal by multiplying the ratio of the particulate isotope activities by the ^{234}Th flux:

$$P_{Be} = \left[^{7}Be/^{234}Th\right]_{particle} P_{Th} \quad (6)$$

Ship time and resource limitations precluded the collection of full ^{234}Th and particle profiles for integration, so a single mixed measurement of ^{234}Th and the particle activity ratio, deemed representative of the mixed layer, was used to estimate the magnitude of ^{7}Be removal. A scavenging depth of 20 m (approximately the mixed layer depth) was used for integration. Results (Table 3) indicate that the removal flux of ^{7}Be from the mixed layer was no greater than 10% of the atmospheric flux determined from the proximate non-upwelling stations (Table 3). Ignoring the upwelling of relatively ^{234}Th enriched deep water to the surface likely leads to an underestimate of P_{Th} by 25–50% (Buesseler et al., 1995). However, there are large uncertainties in the particulate ^{7}Be activities due to the very small signal/noise ratio of the sample peak for these samples. In almost all cases the sample counts were below the limit of detection defined at the 99.7% confidence level, by $>3\sigma_b$, where σ_b is the standard deviation of the blank measurements (Rubinson, 1987). This implies that these calculated removal fluxes are an upper limit. Another approach for evaluating scavenging is to use results from Honeyman and Santchi (1988), which show that the partition

Table 3
^{7}Be and ^{234}Th from the TACE (June 2009) cruise transect across the Equatorial Atlantic.

ML Temp (°C)	Station	Location	Be-7 (ML) particles (dpm/1000 L)	Be-7 (ML) seawater (dpm/1000 L)	(^{7}Be)/(^{234}Th) Particle activity ratio (ML)	(^{234}Th)/(^{238}U) Seawater activity ratio (ML)	Particle removal flux[a]/Input flux
29.11	001	4°39.42′S, 26°49.0′W	bd	837 ± 43	0	1.02 ± 0.04	0
28.95	002	5°01.29′S, 23°00.1′W	160 ± 95	739 ± 41	0.36	1.03 ± 0.03	0
29.0	007	2°31.13′S, 23°00.9′W	bd	597 ± 37	–	NM	0
28.78	011	0°59.528′S, 22 °59.490′W	180 ± 81	369 ± 35	0.21	NM	–
28.10	014	00°00.1 N, 22°58.3′W	bd	343 ± 26	–	0.99 ± 0.02	0
29.0	022	03°0.253′N, 23°0.121′W	bd	556 ± 40	–	NM	0
27.16	064	0°01.679′N, 0°03.801′W	bd	368 ± 41	–	0.97 ± 0.02	0
26.31	035	00°00.5′N, 09°59.4′W	82 ± 63	297 ± 23	0.26	1.05 ± 0.02	0
26.67	051	4°59.642′S, 00°0.063′W	81 ± 72	312 ± 38	0.19	0.87 ± 0.02	0.09
26.96	048	5°00.226′S, 09°59.680′W	134 ± 91	327 ± 36	0.29	0.95 ± 0.02	0.05
25.67	060	0°59.054′S, 0°00.711′E	164 ± 62	270 ± 39	0.34	0.91 ± 0.02	0.11
25.47	056	2°29.99′S, 0°00.92′W	67 ± 48	178 ± 38	0.19	0.85 ± 0.02	0.10

bd = below detection; NM = not measured.

[a] scavenging integrated over 20 m.

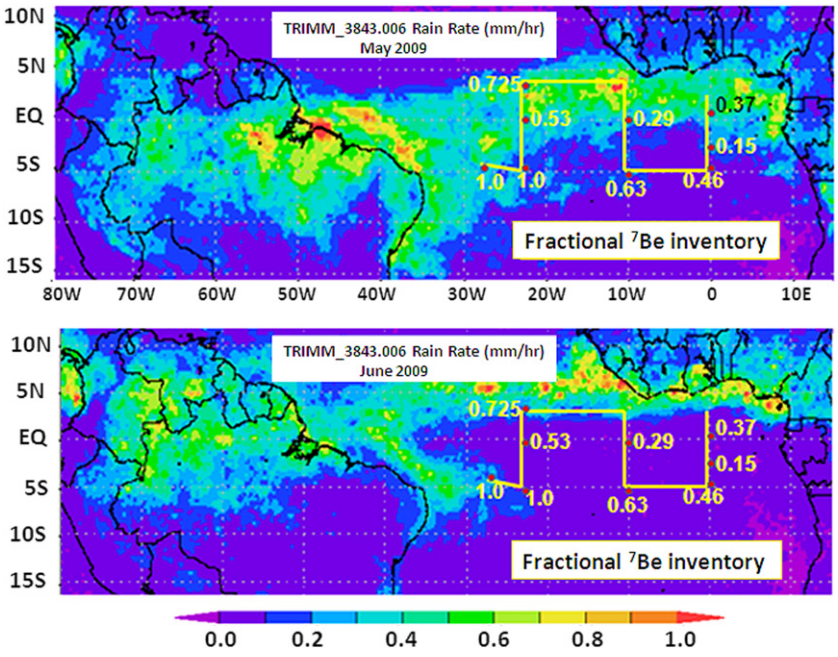

Fig. 7. Station track is superimposed over TRMM rain data for May (top) and June 2009 (bottom). The ^{7}Be inventories, as a fraction of the control flux, $F = 1$, are indicated.

coefficient (adsorbed/dissolved) of Th is an order of magnitude greater than that for Be. However, the longer radioactive half-life of ^{7}Be relative to that of ^{234}Th (2.2) would increase the probability of particle removal for ^{7}Be. The net effect of these factors is to make the fraction of Be lost by scavenging (relative to decay) a factor of about 4.5 less than the fraction of Th lost by particle removal. The ^{234}Th lost by particles is generally less than 10% in these samples, so the fraction of Be lost should be less than 2–3%. Furthermore, as the upwelling rate (w) increases, the flushing of ^{7}Be out of the mixed layer becomes increasingly significant relative to particle removal; for a particle removal rate k_p (d^{-1}), the ratio $H k_p/w$ decreases. Therefore, the large ^{7}Be deficits relative to input (as high as 85%) compared with those of the much more particle reactive ^{234}Th (deficits no greater than 15%) indicate that the significant decrease in ^{7}Be with decrease in mixed layer temperature resulted from dilution with upwelled cold, low ^{7}Be water and not from particle scavenging.

To assess the variability of ^{7}Be flux across the study site we consider the regional rainfall variability, as rain largely controls the delivery of ^{7}Be to the ocean surface. In Fig. 7, the station track is superimposed over Tropical Rainfall Measuring Mission (TRMM) rain data for May and June 2009. It is seen that ^{7}Be inventories are not related to the rain rate (high rain does not correspond to high ^{7}Be inventories). Thus, the trend of decreasing ^{7}Be inventory with decreasing temperature is not caused by variable ^{7}Be delivery. We note that the majority of the stations were occupied in June when the TRMM data indicate relatively uniform rain across the study site. The variable rain observed during May would likely not affect the ^{7}Be inventories measured in June; although the radioactive mean life of ^{7}Be is 77 d, a 20 m mixed layer would be flushed of its ^{7}Be in only 20 d with an upwelling rate of 1 m/d. Thus the system is "reset" on a timescale shorter than one month and the calculated upwelling rates reflect relatively recent and localized conditions.

3.2. One-dimensional diffusion-advection model

To model the vertical profile of ^{7}Be, vertical eddy diffusion, as well as upwelling, must be included. The ^{7}Be concentration in the "tail" layer beneath the mixed layer is governed to first approximation by the one-dimensional vertical advection-diffusion

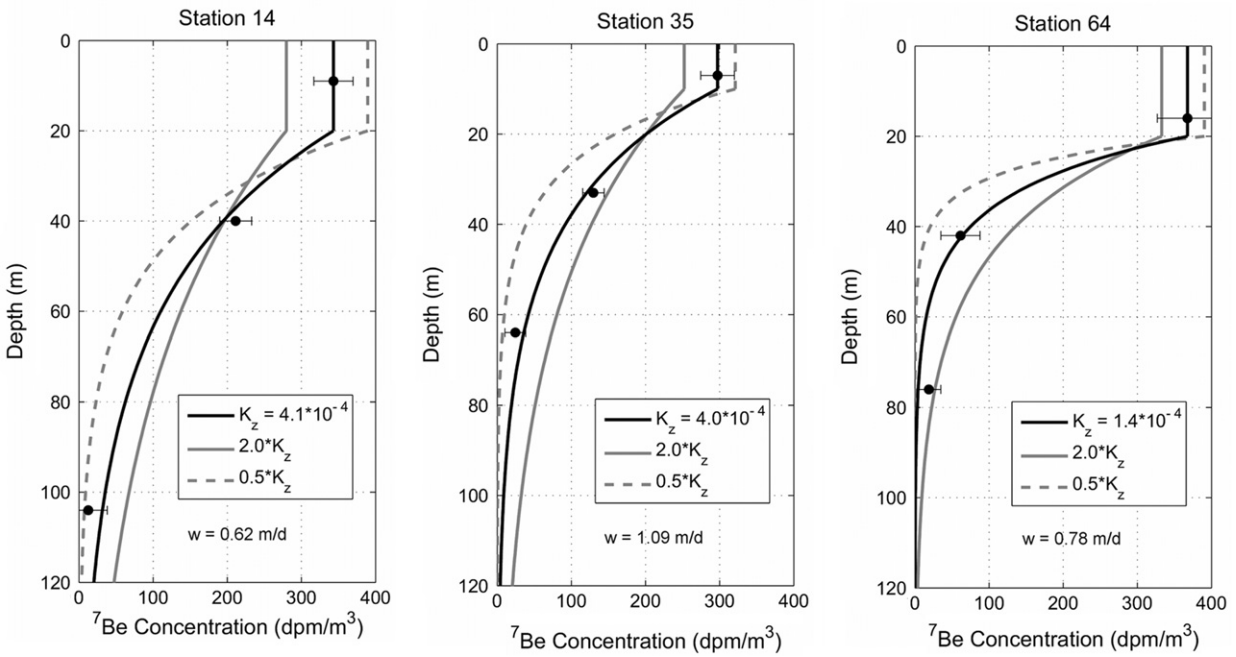

Fig. 8. ^{7}Be profiles at the stations taken along the equator. The data below the mixed layer have been fit to an exponential profile. Using the fitted value of α and the value of w derived for each station from the column inventory method (Eq. (2)), profiles with the required value of K_z are derived. Also shown are ^{7}Be profiles if K_z values of a factor of two greater or smaller are used.

equation, modified by the ^{7}Be decay (see Appendix):

$$\frac{\partial}{\partial z}\left(K_z\frac{\partial C}{\partial z}\right)-\lambda C-w\frac{\partial C}{\partial z}=0 \tag{7}$$

The shape of the ^{7}Be profile below the mixed layer therefore represents a competition between the upwelling, which brings ^{7}Be-depleted water toward the surface, and downward turbulent mixing of high ^{7}Be concentrations from the surface layer. The amount of ^{7}Be found in the "tail" layer thus provides information on the strength of the local vertical mixing. Profiles with a large fraction of the total ^{7}Be inventory contained in the tail layer indicate relatively low upwelling and/or large vertical mixing, whereas those with most of the ^{7}Be inventory confined to the mixed layer indicate either strong upwelling and/or relatively weak mixing.

Assuming constant w (≥ 0) and K_z over the entire ^{7}Be tail layer results in a simple exponential solution for the profile:

$$C(z)=C_0e^{\alpha(z-H)} \tag{8}$$

where the depth attenuation coefficient is given by

$$\alpha=\frac{w}{2K_z}+\frac{1}{2}\left\{\left(\frac{w}{K_z}\right)^2+\frac{4\lambda}{K_z}\right\}^{1/2} \tag{9}$$

Example of ^{7}Be profiles at the three stations taken on the equator (stations 14, 35, and 64) are shown in Fig. 8, where the data below the mixed layer have been fit to an exponential profile. The tail layer fits to an exponential profile quite well and using the fitted value of α and the value of w derived for each station from the column inventory method (Eq. (2), where w is assumed constant through the whole layer), Eq. (9) can be inverted to solve for the required value of K_z. The corresponding K_z values are shown in the legends of Fig. 8, where they range from about 1 to 4×10^{-4} m^2/s. These values are consistent with typical values found in the upper thermocline of the equatorial Atlantic region from microstructure observations (Rhein et al., 2010). Also shown in Fig. 8 are the respective ^{7}Be profiles if K_z values that are a factor of two greater or smaller are used. The ^{7}Be profiles are quite sensitive to the assumed K_z values and provide a fairly strong constraint on the magnitude of the local vertical mixing. The K_z values derived in this manner for all ^{7}Be profile stations are presented in Table 4. A general trend of higher K_z corresponding to higher w is noted.

Table 4
Upwelling model calculations.

Station	W (inventory)[a]	W (slab)[b]	$W_{(100\ m)}$[c]	K_z (10^{-4} m^2/s)[d]
14	0.62	1.06	0.94	4.14
22	0.22	0.37	0.25	0.42
35	1.09	1.40	1.43	4.03
48	0.53	0.67	0.59	0.90
51	0.79	0.93	0.89	0.96
56	2.16	2.28	2.38	1.97
64	0.78	0.97	0.92	1.42

[a] Based on Eq. (2);
[b] Based on Eq. (3);
[c] Based on Eq. (4);
[d] Derived from the one-dimensional diffusion-advection model (Eq. (8)).

As discussed earlier, it is unlikely that the upwelling is constant over the whole depth of the ^{7}Be layer, and it can generally be expected that w decreases with depth below the base of the mixed layer, due to lateral convergence within the upper thermocline (e.g. Wyrtki, 1981). Similarly, the K_z values are likely to be variable in the upper thermocline and are generally expected to decrease with depth as well (e.g. Rhein et al., 2010). Upwelling rates determined from chemical tracers therefore represent an average over the characteristic timescale of the tracer and the depths within the thermocline where the tracer signals are extracted (Wanninkhof et al., 1995); as such, these methods cannot resolve what is likely a complex depth-dependent upwelling pattern (e.g. Harrison, 1996).

In such instances, modeling the ^{7}Be profile for w varying as a function of depth would require solving Eq. (7) numerically. As an example, we show the model results for the case where w decays linearly to zero at a depth of 100 m below the mixed layer (Fig. 9).

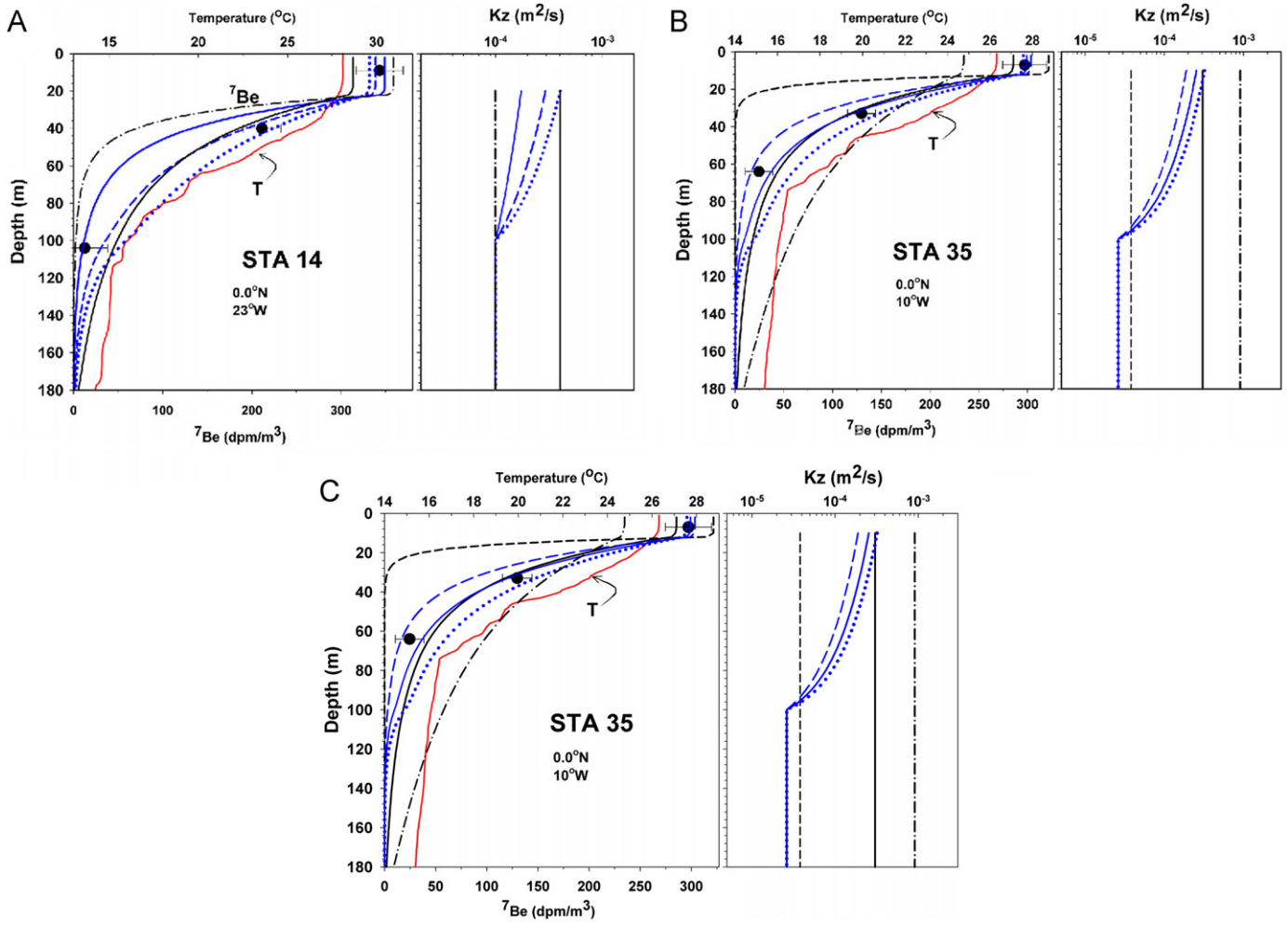

Fig. 9. ^{7}Be profiles at the stations taken along the equator. The data are modeled using the linearly decreasing upwelling velocity shown in Table 4. The left panels show the data and the model profiles generated from the K_z profiles shown in the right panels.

In this case the appropriate value for the upwelling rate at the base of the mixed layer is given by Eq. (4), with z_w set to 100 m (the $W_{(100\ \mathrm{m})}$ column in Table 4). Generally the model results require K_z to decrease with depth as well, consistent with the K_z profiles determined previously from energy dissipation rate measurements from the same general area as our study (Rhein et al., 2010).

4. Summary and conclusions

We have presented the first results using a novel technique, based on the isotope ^{7}Be, to infer rates of upwelling along the equator. The method is based on the dilution of the upper ocean ^{7}Be inventory from penetration of ^{7}Be "dead" water upwelled from below. We calculated the upwelling rates based on three different approaches that were comparable to within 35%. One of these approaches relies only on measurement of the ^{7}Be in the mixed layer, and those estimates were found to agree within about 10% with the estimates based on the most realistic model in which the upwelling is assumed to decay linearly below the mixed layer. The vertical velocity estimates in the cold tongue region varied from about 0.6 to 2.2 m/d, qualitatively consistent with estimates produced from other methods.

To model the vertical profile of ^{7}Be, we used a one-dimensional vertical advection-diffusion equation in which w is assumed to be either constant or linearly decreasing with depth through the upper thermocline. An exponential ^{7}Be profile results in the case of constant w and K_z. The ^{7}Be data were found to fit fairly well to exponential profiles, and yielded corresponding K_z values in the range $\sim$1–4 $\times 10^{-4}$ m^2/s. In the case where w decays linearly to zero at a depth of 100 m below the mixed layer, K_z values are generally required to decrease with depth as well, consistent with the K_z profiles determined previously from energy dissipation rate measurements from the same general area as our study (Rhein et al., 2010). It thus appears that ^{7}Be is a promising new technique for estimating tropical upwelling rates within seasonal timescales.

Acknowledgements

The authors wish to thank the captain and crew of the *R/V Endeavor* for their able field support. Assistance from the University of Miami's Ocean Technology Group in the ^{7}Be sampling and supporting hydrography is gratefully acknowledged. Dr. M. Stephens and Ms. A. Venti provided important at-sea and laboratory technical assistance. We thank Dr. Douglas Hammond and two anonymous reviewers for many helpful comments. This work was supported by the Physical Oceanography and Chemical Oceanography Programs of the NSF, grants OCE-0549522, OCE0623552, and OCE0842785.

Appendix. Mathematical formulation of the ^{7}Be model equations

Equations representing the bulk mixed layer concentration of ^{7}Be and its vertical distribution in the upper thermocline are given by

$$\text{Mixed layer}: H(\partial C_0/\partial t + u\,\nabla C_0) = F - K_z\frac{\partial C}{\partial z}\Big|_H - \lambda C_0 H + w_H(C_H - C_0) \tag{a1}$$

$$\text{“Tail” layer}: \partial C/\partial t + u\,\nabla C = \frac{\partial}{\partial z}\left(K_z\frac{\partial C}{\partial z}\right) - \lambda C - w\frac{\partial C}{\partial z} \tag{a2}$$

where H is the mixed layer depth, and

$$w_H = \partial H/\partial t + \nabla(uH)$$

is the “entrainment” velocity at the base of the mixed layer. Except for the inclusion of the ^{7}Be decay terms, these equations are identical to those commonly used to describe the budgets of conservative properties such as temperature and salinity in the upper ocean (Stevenson and Niiler, 1983; Swensen and Hansen, 1999; Foltz et al., 2003). Here z is positive upwards, so a positive w value corresponds to upwelling. The left hand sides of these equations represent the local rate of change and horizontal advection of ^{7}Be. The terms on the right hand side of (a1) are: the surface flux of ^{7}Be into the mixed layer (F), the downward turbulent flux out of the mixed layer, the ^{7}Be decay, and the entrainment of ^{7}Be into the mixed layer by upwelling and/or mixed layer deepening. The terms on the right hand side of (a2) represent vertical mixing, decay, and vertical advection.

In the entrainment term (the last term of Eq. (a1)), C_H is taken to represent the concentration just below the base of the mixed layer, and is essentially an arbitrary parameter (e.g. Swensen and Hansen, 1999). It can either represent a physical “jump” in the concentration profile, such that upwelling across the base of the mixed layer advects water into the mixed layer with a slightly different concentration than the mixed layer, or represent the average concentration value that is stirred into the mixed layer during mixed layer deepening events. In studies of the surface heat budget, the equivalent temperature value is typically taken to be 1–2 °C cooler than the mixed layer temperature (Wang and McPhaden, 1999). In the present case we expect w_H to be dominated by physical upwelling into the mixed layer along the equator, and if the ^{7}Be profiles are continuous then $C_H = C_0$, and the entrainment term is identically zero. The 2nd and 4th terms in (a1) can be taken together to represent the net vertical flux at the base of the mixed layer, and for reasonable choices of $C_H \geq 0.9C_0$, the entrainment term can be shown to be much smaller than the required mixing flux at the base of the mixed layer (the 2nd term). In practical terms, the choice of C_H does not affect our w_H estimates, since it does not appear explicitly in any of the expressions for w_H derived below for different sets of assumptions.

Assuming a steady state, one-dimensional balance (neglecting horizontal advection), these equations become

$$0 = F - K_z\frac{\partial C}{\partial z}\Big|_H - \lambda C_0 H + w_H(C_H - C_0) \tag{a3}$$

$$0 = \frac{\partial}{\partial z}\left(K_z\frac{\partial C}{\partial z}\right) - \lambda C - w\frac{\partial C}{\partial z} \tag{a4}$$

The presence of a tail layer is indicative of downward mixing from the mixed layer, as in the absence of vertical mixing the ^{7}Be would be confined to the mixed layer with a jump to ^{7}Be = 0 at the base of the mixed layer. In this case (a3) becomes

$$0 = F - \lambda C_0 H - w_H C_0 \tag{a5}$$

When vertical mixing is active, and a tail layer is present, a budget model for the ^{7}Be contained in the entire upper water column can be formed by combining (a3) and (a4). Integrating (a4) from the base of the mixed layer to the depth where the ^{7}Be concentration reaches zero (z_0):

$$0 = K_z\frac{\partial C}{\partial z}\Big|_{z_0}^{H} - \lambda\int_{z_0}^{H} C(z)dz - \int_{z_0}^{H} w\frac{\partial C}{\partial z}dz \tag{a6}$$

Integrating the last term by parts gives

$$0 = K_z\frac{\partial C}{\partial z}\Big|_{z_0}^{H} - \lambda\int_{z_0}^{H} C(z)dz - wC\Big|_{z_0}^{H} + \int_{z_0}^{H} C(z)\frac{\partial w}{\partial z}dz$$

and, noting that both the advective and mixing fluxes tend to zero at z_0:

$$0 = K_z\frac{\partial C}{\partial z}\Big|_H - \lambda\int_{z_0}^{H} C(z)dz - w_H C_H + \int_{z_0}^{H} C(z)\frac{\partial w}{\partial z}dz \tag{a7}$$

Adding (a7) to (a3), after cancellation of terms, then provides the following equation for the total water column from $z = 0$ to z_0:

$$0 = F - \lambda C_{inv} - w_H C_0 + \int_{z_0}^{H} C(z)\frac{\partial w}{\partial z}dz \tag{a8}$$

where C_{inv} is the total water column inventory of ^{7}Be:

$$C_{inv} = \int_{z_0}^{0} C(z)dz = C_0 H + \int_{z_0}^{H} C(z)dz \tag{a9}$$

If w is assumed to be constant between the base of the mixed layer and the depth where the ^{7}Be signal vanishes (typically 60–80 m), then the last term of (a8) is zero and a simple equation results for the upwelling velocity into the mixed layer:

$$w_H = \frac{1}{C_0}(F - \lambda C_{inv}) \tag{a10}$$

If, on the other hand, w is not assumed to be uniform, but is assumed to decay linearly below the mixed layer over a vertical scale z_w, then (a8) yields

$$w_H = (F - \lambda C_{inv})/\left[C_0 - \frac{1}{z_w}\int_{z_0}^{H} C(z)dz\right] \tag{a11}$$

This is the more realistic case, since it is expected that vertical velocity decreases over a finite vertical scale of the order 100 m below the mixed layer (e.g. Harrison, 1996) due to horizontal convergence within the thermocline. In this case the w_H estimate will be somewhat higher than for the uniform upwelling case.

Therefore, there are three different w_H estimates that can be derived from the ^{7}Be data, using Eqs. (a5), (a10), and (a11), depending on the model assumptions. The result from the basic inventory method, Eq. (a10), will always be the lowest of the three estimates, while the result from the simple mixed-layer-only model (the “slab” model, (a5)) is of interest because it relies on only a single measurement of ^{7}Be in the mixed layer.

Finally, if w is assumed to be zero or negligible (i.e. in non-upwelling regions), then from Eq. (a10), the surface flux can be estimated from the water column inventory of ^{7}Be by

$$F = \lambda C_{inv} \tag{a12}$$

which reflects a simple balance between atmospheric flux in the water column and ^{7}Be decay.

References

Aaboe, E., Dion, E.P., Turekian, K.K., 1981. ^{7}Be in Sargasso Sea and Long Island Sound waters. J. Geophys. Res 86, 3255–3257.

Anderson, R.F., Fleer, A.P., 1982. Determination of natural actinides and plutonium in marine particulate material. Anal. Chem. 54, 1142–1147.

Andrews, J.E., Hartin, C., Buesseler, K.O., 2008. ^{7}Be analyses in seawater by low background gamma-spectroscopy. J. Radioanalyt. Nucl. Chem. 277 (1), 253–259.

Bhat, S.G., Krishnaswami., S., Lal, D., Rama, Moore, W.S., 1969. ^{234}Th/^{238}U ratios in the ocean. Earth Planet. Sci. Lett. 5, 483–491.

Broecker, W.S., Peng, T.H., Stuiver, M., 1978. An estimate of the upwelling rate in the Equatorial Atlantic based on the distribution of bomb radiocarbon. J. Geophys. Res. 83, 6179–6186.
Broecker, W.S., Peng, T.-H., 1982. Tracers in the Sea. Eldigio Press, Palisades, New York, U.S.A 690pp.
Bruland, K.W., Coale, K.H., 1986. Surface water ^{234}Th/^{234}U disequilibria spatial and temporal variations of scavenging rates within the Pacific Ocean. In: Burton, J.D., Brewer, P.G., Chesselet, R. (Eds.), Dynamic Processes in the Chemistry of the Upper Ocean. Plenum Press, New York, pp. 159–172.
Buesseler, K.O., Bacon, M.P., Cochran, J.K., Livingston, H.D., 1992. Carbon and nitrogen export during the JGOFS North Atlantic Bloom Experiment estimated from ^{234}Th:^{234}U disequilibria. Deep-Sea Res. 39, 1115–1137.
Buesseler, K.O., Andrews, J.A., Hartman, M.C., Belastock, R., Chai, F., 1995. Regional estimates of the export flux of particulate organic carbon derived from Thorium-234 during the JGOFS EQPAC program. Deep-Sea Res. Part II 42 (2–3), 777–804.
Coale, K.H., Bruland, K.W., 1985. ^{234}Th: ^{234}U disequilibria within the California current. Limnol. and Oceanogr. 30, 22–33.
Coale, K.H., Bruland, K.W., 1987. Oceanic stratified euphoric zone as elucidated by ^{234}Th:^{234}U disequilibria. Limnol. Oceanogr. 32, 189–200.
Foltz, G.R., Grodsky, S.A., Carton, J.A., McPhaden, M.J., 2003. Seasonal mixed layer heat budget of the tropical Atlantic Ocean. J. Geophys. Res. 108 (C5), 3146. doi:10.1029/2002JC001584.
Harrison, D.E., 1996. Vertical velocity in the central tropical Pacific: a circulation model perspective for JGOFS. Deep Sea Res. II 43, 687–705.
Hayes, S.P., Chang, P., McPhaden, M.J., 1991. Variability of the sea surface temperature in the Eastern Equatorial Pacific during 1986–1988. J. Geophys. Res. 96, 10553–10556.
Honeyman, B.D., Santschi, P.H., 1988. Metals in aquatic systems. Environ. Sci. Technol. 22, 862–871.
Kadko, D., Olson, D., 1996. Be-7 as a tracer of surface water subduction and mixed layer history. Deep Sea Res. I 43, 89–116.
Kadko, D., 2000. Modeling the evolution of the Arctic Mixed Layer during the Fall 1997 SHEBA Project using measurements of ^{7}Be. J. Geophys. Res. 105, 3369–3378.
Kadko, D., Swart, P., 2004. The source of the high heat and freshwater content of the upper ocean at the SHEBA site in the Beaufort Sea in 1997. J. Geophys. Res. 109, C01022. doi:10.1029/2002JC001734.
Kadko, D., Johnson, R., 2008Be. Insights into 18 degree mode water formation from measurements of ^{7}Be at the Bermuda Time-Series station. Ocean Sci. Meet. Suppl., Abstr..
Kadko, D., 2009. Rapid oxygen utilization in the ocean twilight zone assessed with the cosmogenic isotope ^{7}Be. Global Biogeochem. Cycles 23, GB4010. doi:10.1029/2009GB003510.
Kadko, D., Prospero, J., 2011. Deposition of ^{7}Be to Bermuda and the regional ocean: environmental factors affecting estimates of atmospheric flux to the ocean. J. Geophys. Res. 116, C02013. doi:10.1029/2010JC006629.
Klein, B., Rhein, M., 2004. Equatorial upwelling rates inferred from helium isotope data: a novel approach. Geophys. Res. Lett. 31, L23308. doi:10.1029/2004GL021262.
Krishnaswami, S., Lal, D., Somayajulu, B.L.K., Dixon, F.S., Stonecipher, S.A., Craig, H., 1972. Silicon, radium, thorium and lead in seawater: in-situ extraction by synthetic fibre. Earth Planet. Sci. Lett. 16, 84–90.
Lal, D., Chung, Y., Platt, T., Lee, T., 1988. Twin cosmogenic radiotracer studies of phosphorus recycling and chemical fluxes in the upper ocean. Limnol. Oceanogr. 336, 1559–1567.
Lee, T., Barg, E., Lal, D., 1991. Studies of vertical mixing in the Southern California Bight with cosmogenic radionuclides 32P and 7Be. Limnol. Oceanogr. 365, 1044–1053.
Lumpkin, R., Garzoli, S.L., 2005. Near-surface circulation in the Tropical Atlantic Ocean. Deep-Sea Res. Part I: Oceanogr. Res. Pap. 52, 495–518. doi:10.1016/j.dsr.2004.09.001.
Matsumoto, E., 1975. ^{234}Th–^{238}U radioactive disequilibrium in the surface layer of the ocean. Geochim. Cosmochim. Acta 39, 205–212.
Quay, P.D., Stuiver, M., Broecker, W.S., 1983. Upwelling rates for the equatorial Pacific Ocean derived from the bomb ^{14}C distribution. J. Mar. Res. 41, 769–792.
Rhein, M., Dengler, M., Sültenfuß, J., Hummels, R., Hüttl-Kabus, S., Bourles, B., 2010. Upwelling and associated heat flux in the equatorial Atlantic inferred from helium isotope disequilibrium. J. Geophys. Res. 115, C08021 10.1029/2009C005772.
Rubinson, K.A., 1987. Chemical Analysis. Little, Brown and Co., Toronto, pp. 754–758.
Silker, W.B., 1972. Beryllium-7 and fission products in the GEOSECS II water column and applications of their oceanic distributions. Earth Planet. Sci. Lett. 16, 131–137.
Stevenson, J.W., Niiler, P.P., 1983. Upper ocean heat budget during the Hawaii-to-Tahiti shuttle experiment. J. Phys. Oceanogr. 13, 1894–1907.
Swenson, M.S., Hansen, D.V., 1999. Tropical Pacific ocean mixed layer heat budget: the Pacific cold tongue. J. Phys. Oceanogr. 29, 69–81.
Wang, W.M., McPhaden, M.J., 1999. The surface-layer heat balance in the equatorial Pacific Ocean. Part I: mean seasonal cycle. J. Phys. Oceanogr. 29, 1812–1831.
Wanninkhof, R., Feely, R.A., Atwood, D.K., Berberian, G., Wilson, D., Murphy, P.P., Lamb, M.F., 1995. Seasonal and lateral variations in carbon chemistry of surface water in the eastern equatorial Pacific during 1992. Deep-Sea Res. II 42, 387–409.
Weinstein, S.E., Moran, S.B., 2005. Vertical flux of particulate Al, Fe, Pb, and Ba from the upper ocean estimated from ^{234}Th/^{238}U disequilibria. Deep-Sea Res. I 52, 1477–1488.
Wyrtki, K., 1981. An estimate of equatorial upwelling in the Pacific. J. Phys. Oceanogr. 11, 1205–1214.
Young, J.A., Silker, W.B., 1980. Aerosol deposition velocities on the Pacific and Atlantic Oceans calculated from ^{7}Be measurements. Earth Planet. Sci. Lett. 50, 92–104.
Xie, L., Hsieh, W.W., 1995. The global distribution of wind-induced upwelling. Fish. Ocean 4 (1), 52–67.